International Journal of Engineering and Applied Sciences (IJEAS)
Vol.1, Issue 1(2009)1-18

BALLISTIC IMPACT OF 3D ORTHOGONAL WOVEN COMPOSITE BY A SPHERICAL BULLET: EXPERIMENTAL STUDY AND NUMERICAL SIMULATION

Y.M. Yu[1,2], X.J. Wang[2] and C.W. Lim[1]
[1]Department of Building and Construction, City University of Hong Kong, Tat Chee Avenue, Kowloon, Hong Kong
[2]Department of Modern Mechanics, University of Science and Technology of China, Hefei, Anhui, China, 230027

Accepted Date: 18 April 2009

Abstract

A ballistic impact experiment and numerical simulation study of Kevlar/Vinyl and E-glass/Vinyl 3D orthogonal woven composite by a spherical bullet is presented in this paper. The experiment shows that the ballistic performance of Kevlar29/Vinyl is better than E-glass/Vinyl 3D orthogonal woven composite. The analysis of damage modes points out that compression/shear failure mechanism occurs on the front side while tensile failure on the back side. The existence of Z yarns is the main cause of in-plane energy absorption mechanism. In numerical simulation, the orthogonal isotropic constitutive equation with damage tensor and Hashin failure criterion are adopted. Simulation of the penetration process is presented and the residual velocity calculated is fitted to the experimental values. Finally, the details of damage evolution of x-direction fibers and in-plane matrix are studied.

Keywords: 3D orthogonal woven composite, ballistic impact, ballistic limit, damage evolution, E-glass, Hashin failure criterion, Kevlar

1. Introduction

Fiber-reinforced composites are widely used in aerospace and armor protection in military applications. The 3D orthogonal woven composite (3D-OWC in brief) contains not only the in-plane perpendicularly stacked warp yarns and weft yarns, but also the Z yarns along the thickness direction [1], see Fig. 1. The Z yarns run through the in-plane fiber layers from top to bottom to form a 3D structure which inhibit the expanding of interlamination crack and enhance the damage tolerance, as compared to laminates [2,3]. Tan et al. [4-8] did a series of thermo-mechanical experiments about CFRP and GFRP, and established a unit cell for FEM analysis. Tong et al. [9], Shahkarami et al. [10] considered the effect of yarn waviness and established a more authentic beam model and shell model, respectively, to analyze the mechanical properties. Rudov-Clark et al. [11] discussed the tensile fatigue properties of 3D orthogonal woven composite, and found that the fatigue life and residual strength are lower than that of a 2D woven composite, and they decreased with increasing z-binder content.

Callus et al. [12] conducted tensile experiment of three kinds of 3D woven GRP composites and studied the failure mechanism. Quinn et al. [13] studied the failure modes of 3D orthogonal woven composite in tension by using electronic speckle pattern interferometer. Lv et al. [14-16] performed SHPB experiments on 3D Orthogonal Hybrid Woven Composite to analyze the strain rate sensitivity of energy absorption and discussed the damage modes under quasi-static and impact loading, and implemented FEM simulation in ABAQUS by a unit-cell model. Naik et al. [17-20] studied the ballistic impact behaviors of woven fabric composites, and analyzed the energy absorption mechanism and established an energy model. Karim [21] presented various kinds of constitutive modeling and failure criteria of carbon-fiber reinforced polymers in his doctoral studies. Tan et al. [22] presents an FE model of woven fabric that reflects the orthotropic properties of the fabric, the viscoelastic nature of yarns, the crimping of yarns, the sliding contact between yarns and yarn breakage using an assembly of viscoelastic bar elements. Gama et al. [23, 24] employed a finite element model of the unit cell by using fabric design and processing parameters of a 3D orthogonal weave composite to compute effective elastic properties of the unit cell model. They studied the impact, damage, penetration, and energy absorption of such 3D woven composites.

Although many research works on 3D orthogonal woven composites have been reported recently, there are still plenty of rooms for further development, particularly the mechanical properties related to the fiber categories, fiber volume fraction and other effective factors are yet fully understood. In this paper, experiments of Kevlar29/Vinyl and E-glass/Vinyl 3D orthogonal woven composites subject to an impact by a spherical bullet are conducted to study their ballistic performance and energy absorption mechanism. Numerical simulations are also presented to investigate the damage evolution of 3D orthogonal woven composite.

2. Experimental Investigation

The materials of targets for ballistic experiment are Kevlar29/Vinyl and E-glass/Vinyl with Kevlar29 or E-glass as the fibers and Vinyl as the matrix. They are 3D orthogonal woven composites with densities 1.29g/cm^3 and 1.89g/cm^3, respectively. The coarseness of warp yarns, weft yarns, and Z yarns are 628Tex, 628Tex, 314Tex (1Tex=1g/1000m), respectively, for both targets. The weaving tightness of warp and weft yarns are both 40 bundles per 10cm. The fabric volume factions for these targets are 60%, with 10% Z fibers volume faction, and the thickness are 3.5mm, 4.5mm, and 8.5mm for these targets. The spherical bullet is made of 45 # steel (0.45% carbon steel) with a diameter of 5.0mm. A sample of Kevlar29/Vinyl 3D orthogonal woven composite is shown in Fig. 2.

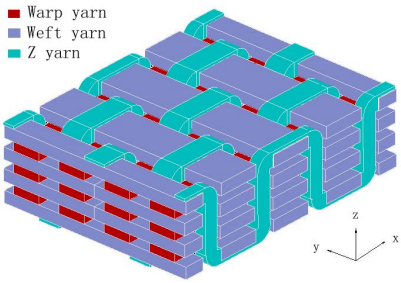

Fig.1. Sketch of 3D-OWC

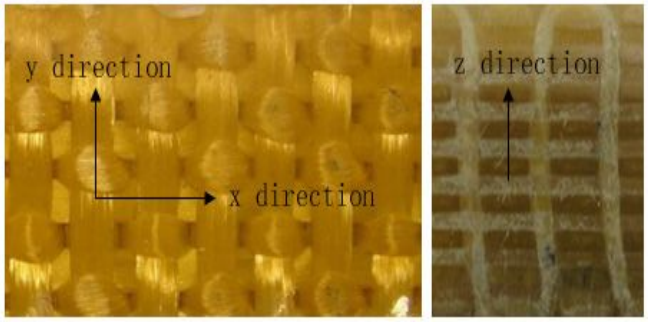

Fig.2. Sample of Kevlar29/Vinyl 3D-OWC

The ballistic experiment setup is illustrated in Fig. 3. A bullet is ejected from the bore at point A with a high speed, runs through the front laser timer which measures the bullet's velocity at point B, V_B. It then moves forward, impacts the target with an incident velocity $V_i < V_B$, penetrates and leaves the target with a residual velocity $V_r < V_i$. It continues moving ahead and runs through the back laser timer which measures the velocity at point D, $V_D < V_r$.

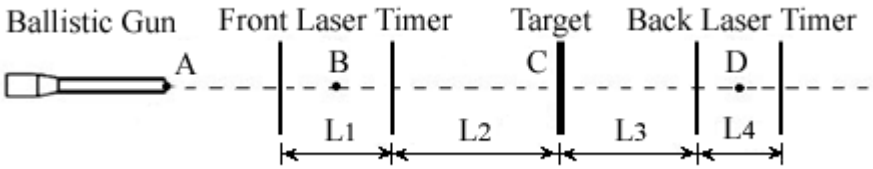

Fig.3. Sketch of ballistic experiment

Because of air resistance, the bullet velocity degrades while moving in the air. The following empirical equation for velocity attenuation

$$V_x = V_0 e^{-0.011x} \tag{1}$$

can be applied, in which $V_D < V_r$ are approximated from V_B and V_D, respectively. The distance L_1, L_2, L_3, L_4 are known from the experiment.

3. Results and Analysis

3.1 Relationship of V_i and V_r

The relation between the incident velocity V_i and the residual velocity V_r is presented in Fig. 4. Each impact velocity in the figure is an average of three effective shootings. All V_i-V_r relations are linear lines nearly parallel to a straight line inclining at

45° to the horizontal, ie. the linear line $y = x$. This result is unanimous due to the fact that $y = x$ is an asymptote for the V_i-V_r lines when V_i is far higher than the ballistic limit.

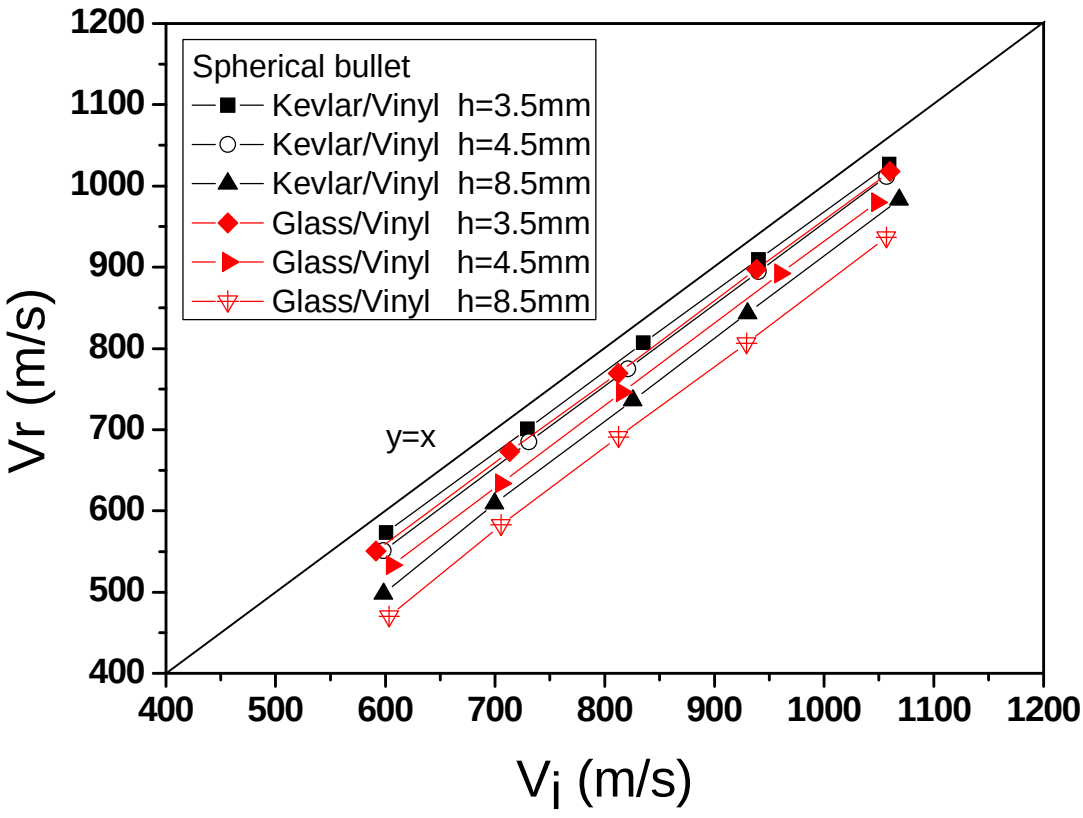

Fig.4. Relationship of V_i and V_r.

For a rigid bullet, the energy conservation law gives,

$$\frac{1}{2}M_b V_i^2 = \frac{1}{2}M_b V_r^2 + \frac{1}{2}M_b V_{50}^2 \qquad (2)$$

where M_b is the bullet mass and V_{50} is the ballistic limit with 50% penetration probability. From Eq. (2), the following equation

$$V_r / V_i = \sqrt{1-(V_{50} / V_i)^2} \qquad (3)$$

can be obtained. If $V_i \gg V_{50}$, then $V_r / V_i \to 1$. As a result, the linear line $y = x$ is an asymptote of the V_i-V_r lines.

When a spherical bullet impacts on the targets with identical V_i and thickness, the V_r of E-glass/Vinyl is lower than that of Kevlar29/Vinyl. It means that the former absorbs more bullet kinetic energy than the latter. However this does not imply that the

anti-penetration performance of E-glass/Vinyl is better than that of Kevlar29/Vinyl. The readers are referred to the following section on the penetration performance of a target for further details.

3.2 Ballistic Limit V_{50} and Ballistic Performance Index (BPI)

Ballistic limit is used to describe the relation between bullet impact velocity and penetration possibility. It evaluates the capability of anti-penetration of targets. The velocity with 50% penetration possibility, ie. V_{50}, is used widely. In the experiment, the Langlie shooting method is adopted. The result is presented in Table.1.

Table 1. V_{50} for different targets by a spherical bullet

Target	Kevlar/vinyl 3D-OWC			E-glass/Vinyl 3D-OWC		
Thickness (mm)	3.5	4.5	8.5	3.5	4.5	8.5
V_{50} (m/s)	185	231	342	213	252	349

The ballistic performance index (*BPI*)

$$BPI = \frac{EA}{AD} \tag{4}$$

is used to compare the ballistic performance of different targets regardless of the effect of thickness or density. It equals to the energy absorbed per area density of target. Materials with higher *BPI* have better ballistic performance, and they can absorb more energy when they are impacted by a bullet. In Eq. (4), EA is the energy absorbed by target while AD is the target area density, the product of target density and its thickness.

In the experiment, no deformation of bullet is observed. It is then valid that the energy absorbed by the target equals to the loss of bullet kinetic energy

$$EA = \frac{1}{2} M_b V_i^2 - \frac{1}{2} M_b V_r^2 \tag{5a}$$

or equivalently the kinetic energy for an impact at the ballistic limit V_{50}.

$$EA = \frac{1}{2} M_b V_{50}^2 \tag{5b}$$

Using the experimental V_{50}, the relation between EA and AD can be obtained as shown in Fig. 5. Obviously, the slope of the EA - AD line, namely the *BPI*, for Kevlar/Vinyl is higher than that of E-glass/Vinyl. It implies that the former has better ballistic performance than the latter disregard of the conclusion in Sec. 3.1 that E-glass/Vinyl absorbs more energy than Kevlar/Vinyl in the case of identical target thickness.

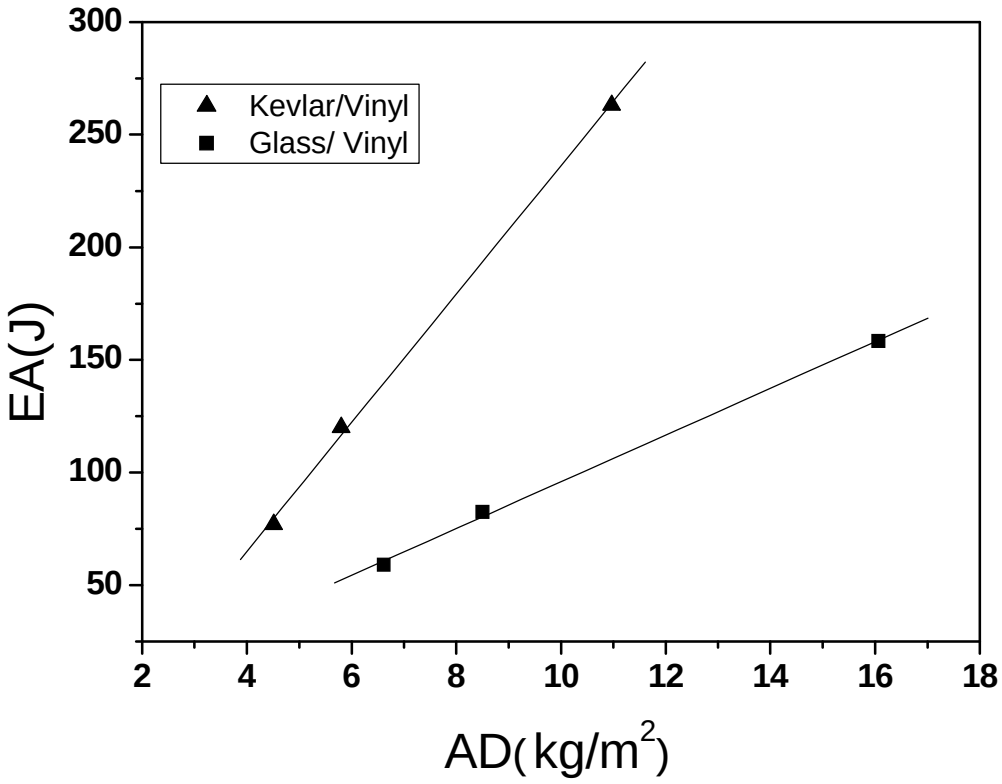

Fig.5. *EA - AD* relationship

4. Damage Modes and Energy Absorption Mechanism

4.1 Damage modes

To analyze the damage modes of 3D orthogonal woven composite, an example of impact of E-glass/Vinyl with thickness 8.5mm by a spherical bullet at the velocity of ballistic limit is shown in Fig. 6. On the impact side, the target is badly destroyed within an area of twice the diameter of the bullet. Away form the center, there are many matrix crack circles as observed in Fig. 6 (a). At the center of the bullet hole, the vinyl matrix is broken off. The E-glass fibers are sheared by the bullet, leaving a regular incision, see Fig. 6 (b). It indicates that compression and shearing are the main failure causes on the impact side.

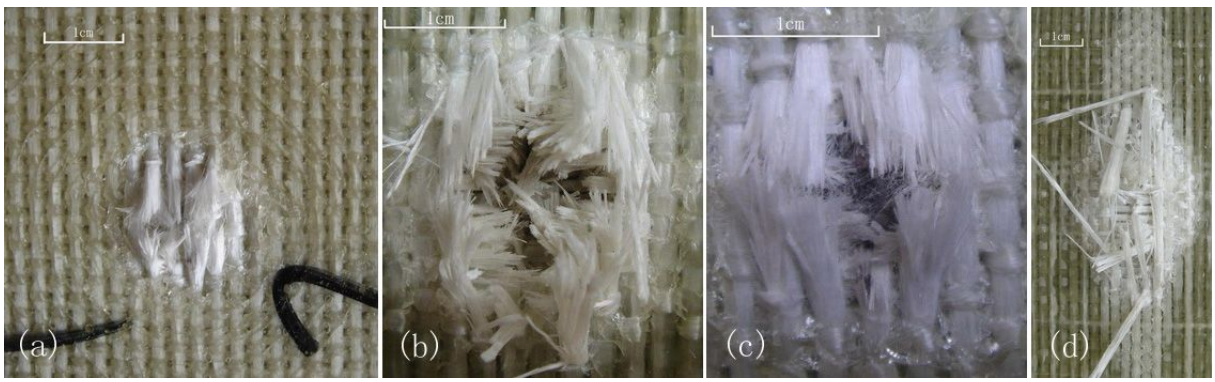

Fig. 6. Damage pattern (a) Damage on front face (b) Front face (c) Back face (d) Damage on back face

On the back side, the fibers are broken due to excessive tension. The matrix damage is similar to that of the impact side, see Fig. 6(c). Hence, tensile failure is the main failure mechanism of 3D orthogonal woven composite on the back side. The damage area is obviously observed in Fig. 6(d).

Comparing to classical lamimates, the failure characteristics of the 3D orthogonal woven composite after the impact by a spherical bullet show the following:

- the back side dose not have obvious bulge;
- no delamination;
- the damage area is much smaller.

4.2 Energy absorption mechanism of 3D-OWC

The main energy absorption mechanisms for fabric composites include in-plane and off-plane energy absorption, and delamination energy absorption.

A. In-plane and off-plane energy absorption

Upon the impact of a high speed bullet on the fabric composite, two shock waves propagating in the composite occur, ie. the longitudinal wave along the fiber of yarns and the transversal wave along the moving direction of bullet, see Fig. 7. For the longitudinal wave, it moves at a specific wave velocity results in more sections of the yarn to deform or even to fail. The strain energy or fracture consumes part of the bullet kinetic energy. This is called the in-plane energy absorption.

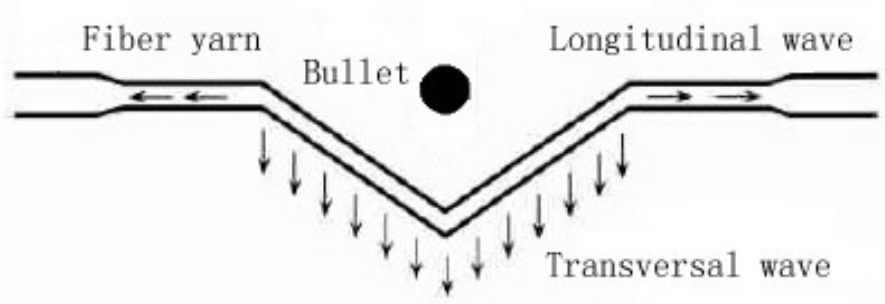

Fig.7. Longitudinal and transverse wave

The warp and weft yarn layers, which are perpendicularly stacked to each other, have lots of crossing points. The adjacent layers interact through these crossing points and the matrix. The transverse wave propagates along the thickness direction. It causes transverse displacement to those fibers that are not in contact with the bullet and a conical bulge is then created. The interaction of longitudinal wave results in transverse movement of more crossing points and fibers and the conical bulge becomes bigger. Consequently, the bullet either penetrates through the target or is blocked by it. The transverse movement of fibers consumes another portion of the bullet kinetic energy, and it is called the off-plane energy absorption.

Assuming the target with elastic fibers is impacted by a bullet with velocity v, then the relation between transverse wave velocity u, longitudinal wave velocity c, bullet velocity v and longitudinal strain of fiber e can be expressed as

$$c = \sqrt{E / r} \tag{6}$$

$$u = c\left(\sqrt{e\left(1+e\right)} - e\right) \tag{7}$$

$$v = c\sqrt{2e\sqrt{e\left(1+e\right)} - e^2} \tag{8}$$

where E is Young's Modulus of fiber and r is the density of fiber.

From Eqs. (6)-(8), the longitudinal wave velocity is high for fiber with high modulus and low density. It implies that the target absorbs more energy because longitudinal strain exists in more fiber sections. On the other hand, the high transverse wave velocity yields high transverse motion of more crossing points, which in turn cause more off-plane energy absorption and bigger conical bulge.

In the experiments, the Young's moduli of Kevlar29 fiber and E-glass fiber are 70Gpa and 73Gpa, and the densities are 1.44g/cm3 and 2.54g/cm3, respectively. With impact by the same spherical bullet, the longitudinal wave velocity for Kevlar29 is higher than that for E-glass. Hence, more fibers in Kevlar29/Vinyl absorb energy. This is the inherent reason the ballistic performance of Kevlar/Vinyl is better than that of E-glass/ Vinyl 3D-OWC.

Because there is no obvious bulge on the back side of the targets, the off-plane energy absorption mechanism is not the main cause in this process. As a result, the Z yarns play an important role. The Z yarns run through the 3D structure and constrain the transverse movement of fibers. Consequently, the in-plane energy absorption mechanism is the main process for 3D orthogonal woven composite when it is impacted by a bullet.

B. Delamination energy absorption

It is known that the transverse compressive wave velocity is much higher than the bullet velocity, the compressive wave reaches the back side and reflects to yield a tensile wave before the bullet penetrates the target. Delamination of target may occur when the strength of tensile wave is higher than the interface strength. The delamination caused by tensile stress is called Mode 1 delamination. Meanwhile, during bullet penetration, another Mode 2 delamination caused by in-plane shear stress may occur, see Fig. 8. Delamination between layers is one of the main energy absorption mechanisms because it absorbs bullet energy during impact.

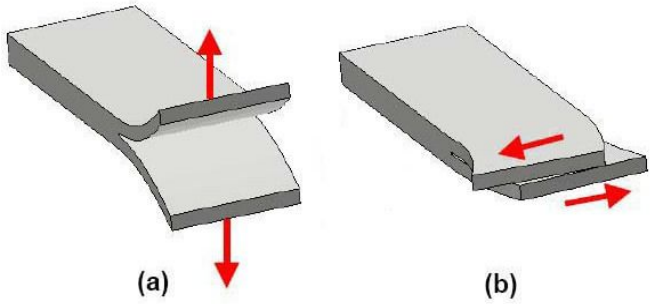

Fig. 8. Delamination modes, (a) Mode 1; (b) Mode 2

Generally speaking, low interface tensile strength leads to Mode 1 delamination while low interface shearing strength leads to Mode 2 delamination. Unlike laminates whose

interface strength is determined by matrix or the bond strength between the matrix and fibers, the interface strength of 3D orthogonal woven composite is determined by the Z yarns. The relatively high tensile strength and shear strength of Z yarns, comparing to the laminates, is able to constraint the delamination crack evolution effectively in the 3D-OWC. These agree with the experiment observation that there exists no delamimation mode. Hence, delamination energy absorption is very limited for 3D orthogonal woven composite.

5. Numerical Simulation

5.1 Modeling of bullet

A standard finite element model for the bullet is described here. The Gruneisen state equation [25] and the strain rate effect considered in the Johnson-Cook strength model [25] are adopted for the bullet. The keywords in LS-Dyna [26] are *EOS_GRUNEISEN and *MAT_JOHNSON_COOK, respectively. The Gruneisen state equation is

$$p=\frac{r_0C^2m\left[1+\left(1-\frac{g_0}{2}\right)-\frac{a}{2}m^2\right]}{1-(S_1-1)m}+(g_0+am)E \tag{9}$$

where r_0 is the initial density; C, S_1 are intercept and coefficient of the Hugoniot curve, respectively; g_0 the Gruneisen Gamma; a the first-order volume correction to g_0 and $m=r/r_0-1$. The Johnson-Cook equation is

$$s_y=\left(A+B\bar{e}^{p^N}\right)\left[1+c\ln\left(\dot{\bar{e}}^p/\dot{\bar{e}}_0\right)\right]\left[1-\left(\frac{T-T_{room}}{T_{melt}-T_{room}}\right)^m\right] \tag{10}$$

where A, B, N, c, m are simulation parameters of the constitutive equation; T_{melt}, T_{room} are the material melting temperature and ambient room temperature, respectively; $\dot{\bar{e}}^p$ the effective plastic strain rate; and the reference strain rate $\dot{\bar{e}}_0=1\,\text{s}^{-1}$ is adopted. The standard parameters for 45 steel are listed in Tables 2 and 3.

Table 2. Parameters of Gruneisen EOS of bullet

r_0 (kg/m^3)	C (m/s)	S_1	g_0	a
7830	4569	1.49	2.17	0.46

Table 3. Parameters of Johnson-Cook of bullet

G (GPa)	A (MPa)	B (MPa)	N	C	m	T_{melt} (K)	T_{room} (K)
77	792	510	0.26	0.014	1.03	1793	294

5.2 Modeling of Kevlar29/Vinyl 3D orthogonal woven composite

5.2.1 Orthogonal anisotropic constitutive

Due to orthogonal anisotropy and damage diversity of composite, an orthogonal anisotropic constitutive relation is adopted. It includes the damage tensor w_i $(i=1,2,\mathbf{K},6)$ to reflect the mechanical properties of 3D orthogonal woven composite. It is obvious that w_i represents material weakness. The elastic constants in the constitutive equation are listed in Table 4.

$$\begin{Bmatrix} e_1 \\ e_2 \\ e_3 \\ e_4 \\ e_5 \\ e_6 \end{Bmatrix} = \begin{bmatrix} \frac{1}{(1-w_1)E_1} & -\frac{n_{21}}{E_2} & -\frac{n_{31}}{E_3} & 0 & 0 & 0 \\ -\frac{n_{12}}{E_1} & \frac{1}{(1-w_2)E_2} & -\frac{n_{32}}{E_3} & 0 & 0 & 0 \\ -\frac{n_{13}}{E_1} & -\frac{n_{23}}{E_2} & \frac{1}{(1-w_3)E_3} & 0 & 0 & 0 \\ 0 & 0 & 0 & \frac{1}{(1-w_4)G_{12}} & 0 & 0 \\ 0 & 0 & 0 & 0 & \frac{1}{(1-w_5)G_{23}} & 0 \\ 0 & 0 & 0 & 0 & 0 & \frac{1}{(1-w_6)G_{31}} \end{bmatrix} \begin{Bmatrix} s_1 \\ s_2 \\ s_3 \\ s_4 \\ s_5 \\ s_6 \end{Bmatrix} \tag{11}$$

Table 4. Elastic constants of Kevlar29/Vinyl 3D-OWC

E_1 (GPa)	E_2 (GPa)	E_3 (GPa)	n_{21}	n_{31}	n_{32}	G_{12} (GPa)	G_{23} (GPa)	G_{31} (GPa)
18.4	18.4	10.2	0.14	0.08	0.08	8.0	8.0	4.7

5.2.1 Hashin failure criterion

In this paper, the Hashin failure criterion [25] is used. This criterion is commonly used in composite damage simulation because different loads lead to different failure modes. The keyword for the Hashin failure criterion in LS-Dyna is *MAT_COMPOSITE_DMG_MSC. There are seven types of damage that can be divided into four categories as follows [26]:

1). Tensile/shear damage of fibers

$$x \text{ direction:} \quad f_1 = \left(\frac{\hat{E}_1 \langle e_1 \rangle}{S_{1T}} \right)^2 + \left(\frac{\hat{G}_{31} e_{31}}{S_{1FS}} \right)^2 - r_1^2 = 0 \tag{12}$$

$$y \text{ direction:} \quad f_2 = \left(\frac{\hat{E}_2 \langle e_2 \rangle}{S_{2T}} \right)^2 + \left(\frac{\hat{G}_{32} e_{32}}{S_{2FS}} \right)^2 - r_2^2 = 0 \tag{13}$$

2). Compressive damage of fibers

$$x \text{ direction:} \quad f_3 = \left(\frac{\hat{E}_1 \langle -e_1^{'} \rangle}{S_{1C}} \right)^2 - r_3^2 = 0, \qquad e_1^{'} = e_1 + e_3 \frac{E_3}{E_1} \tag{14}$$

$$y \text{ direction:} \quad f_4 = \left(\frac{\hat{E}_2 \langle -e_2^{'} \rangle}{S_{2C}} \right)^2 - r_4^2 = 0, \qquad e_2^{'} = e_2 + e_3 \frac{E_3}{E_2} \tag{15}$$

$$z \text{ direction:} \quad f_5 = \left(\frac{\hat{E}_3 \langle -e_3 \rangle}{S_{3C}} \right)^2 - r_5^2 = 0 \tag{16}$$

3). In-plane damage of Matrix

$$f_6 = \left(\frac{\hat{G}_{12} e_{12}}{S_{12}} \right)^2 - r_6^2 = 0 \tag{17}$$

4). Transversal Damage of Matrix

$$f_7 = \left(\frac{\hat{E}_3 \langle e_3 \rangle}{S_{3T}} \right)^2 + \left(\frac{\hat{G}_{23} e_{23}}{S_{23}} \right)^2 + \left(\frac{\hat{G}_{31} e_{31}}{S_{31}} \right)^2 - r_7^2 = 0 \tag{18}$$

The readers are referred to the manual of LS-DYNA [26] for further details.

Damage surface f_j $(j = 1, 2, \mathbf{K}, 7)$ is a quadratic surface in strain space. It is a discriminant that governs the damage calculation. The area surrounded by the damage surface corresponds to a material state with a given damage or no damage, while the area outside relates to a state with damage evolution. The evaluation of damage surface is $r_j \geq 1$ where $r_j = 1$ is the threshold for damage calculation.

In the equations above, S_{1T}, S_{2T}, S_{3T} are tensile strength along the *x*-, *y*-, *z*-directions, respectively; S_{1C}, S_{2C}, S_{3C} are the corresponding compression strength; S_{12}, S_{23}, S_{31} the shear strength in *xy*-, *yz*-, *zx*-planes, respectively; S_{1FS}, S_{2FS} the Layer shear strength due to fiber shear failure in *x*-, *y*-directions, respectively; $\hat{E}$, $\hat{G}$ the effective Young's modulus and shear modulus considering damage tensor, respectively, ie. $\hat{E}_1 = (1 - w_1) E_1$, $\hat{G}_1 = (1 - w_1) G_1$ where $\langle \ \rangle$ is the Macaulay bracket. The parameters in Eqs. (12)-(18) are listed in Table 5.

Table 5. Strength parameters of Kevlar/Vinyl 3D-OWC (MPa)

S_{1T}	S_{1C}	S_{2T}	S_{2C}	S_{3T}	S_{3C}	S_{1FS}	S_{2FS}	S_{12}	S_{23}	S_{31}
420	160	360	140	200	480	240	206	180	180	180

5.2.3 Damage evolution calculation

Considering the coupling effect of different damage modes, the damage evolution rate can be expressed as,

$$\dot{w}_i = \sum_j f_j q_{ij} \tag{20}$$

where q_{ij} is the coupling tensor and it represents the contribution of damage mode j to the damage quantity w_i. Taking w_1 for example, $q_1 = \{1\ 0\ 1\ 0\ 1\ 0\ 0\}^T$; f_j is the evolution rate of single damage mode j described in Eqs. (13)-(19). The damage will accumulate or develop only when the strain rate $\dot{\varepsilon}_j$ has a nonnegative component along the normal direction of damage surface. Otherwise, the damage state will remain unchanged [26]. The function f_i can be expressed as

$$f_i = \sum_j g_i \frac{\partial f_i}{\partial e_j}\dot{\varepsilon}_j \quad (i\text{:no sum}) \quad \left(\text{only when } \frac{\partial f_i}{\partial e_j}\dot{\varepsilon}_j > 0\right) \tag{21}$$

where $g_i = f_i^{n-1}$ is a parameter to describe evolution speed of damage mode i [27].

6. Simulation Results and Analysis

6.1 Residual velocity V_r

The comparison of residual velocity V_r between ballistic experiment and numerical simulation for Kevlar29/Vinyl can be seen in Fig. 9. The numerical results are fitted to the experimental value and general agreement is observed. In general, discrepancy of experiment and numerical simulation increases with increasing incident velocity V_i with a maximum error of 3.68%. The increasing disagreement is believed mostly due to greater velocity and measurement uncertainties.

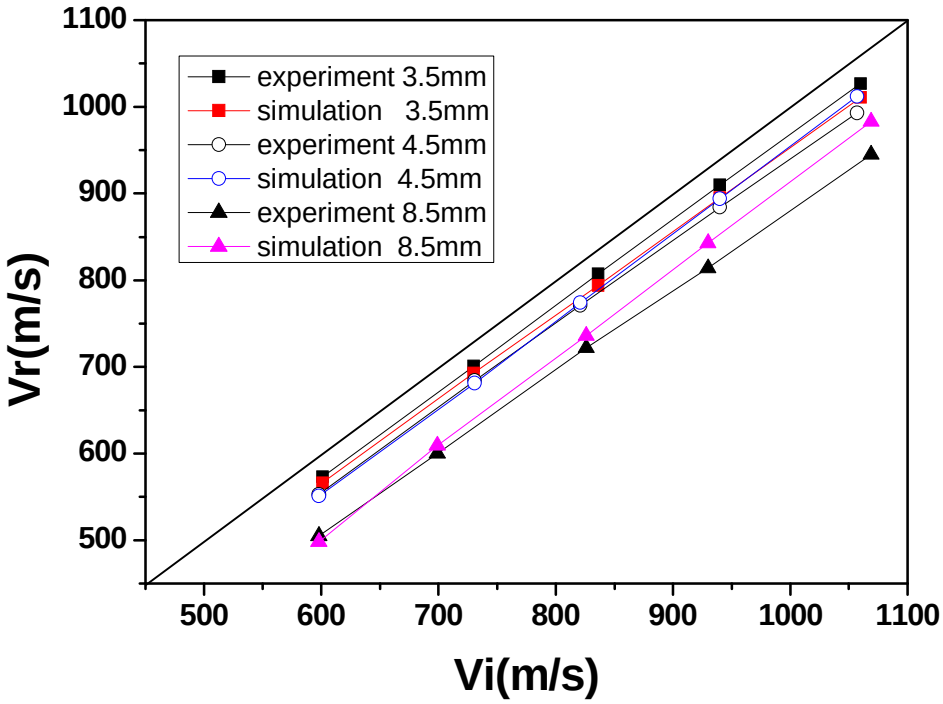

Fig. 9. Simulating residual velocity of targets of diff. thickness.

6.2 Time history of penetration velocity V_p

The penetration velocity V_p is an important concept in penetration mechanics. It relates the penetration law and the ultimate penetration depth of the bullet. Because the time history of penetration velocity is impossible to be measured in experiment, numerical simulation becomes the effective mean. For convenience, V_p / V_i is adopted as the dimensionless penetration velocity while the time in ms is denoted as t. For illustration, an example of 8.5mm target is presented in Fig. 10.

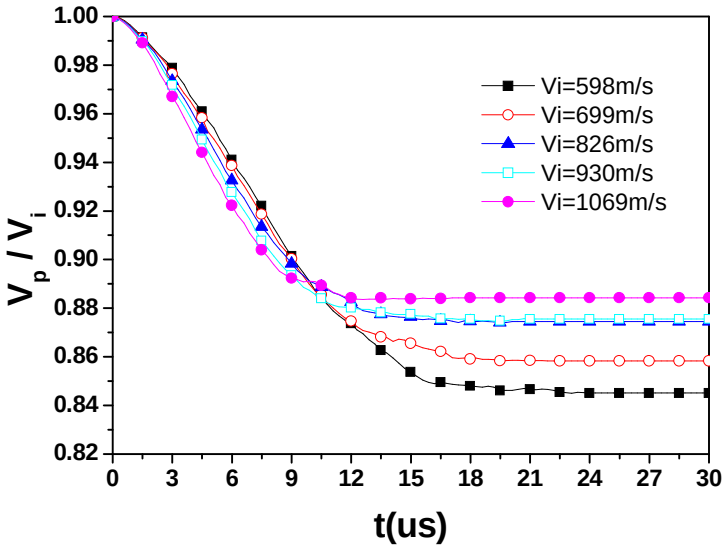

(a) Time history of penetration velocity

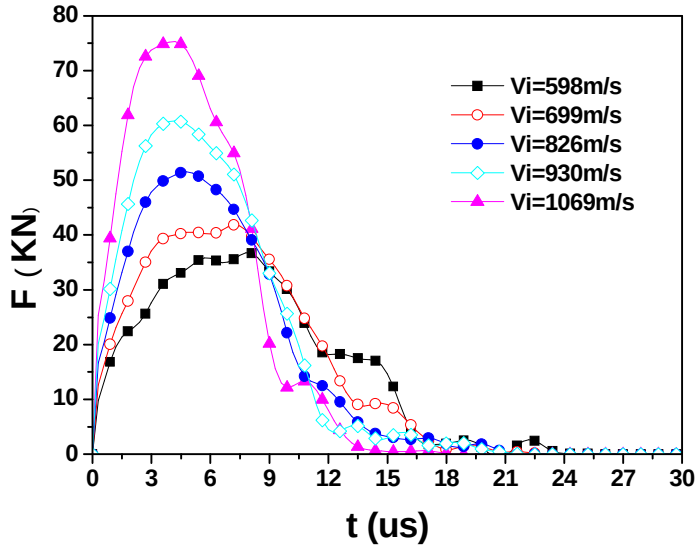

(b) Loads history of bullet in penetration

Fig. 10. Time history of (a) penetration velocity; and (b) loads.

At the early stage of penetration, the bullet velocity degrades nearly linearly, which implies constant acceleration, ie. a state of steady penetration, see Fig.10 (a). Figure 10 (b) shows that there exists a finite period of time at the peak load which corresponds to a period of steady penetration. This finite steady period decreases as V_i increasing. As penetration progresses, the velocity, resistance, and acceleration decrease until the bullet leaves the target with a stable, residual velocity V_r.

6.3 Damage evolution

In LS-Dyna, the evolution of damage is reflected by the history variables. There are six kinds of damage history variables in *MAT_COMPOSITE_DMG_MSC: the damage of *x*–fiber; the damage of y-fiber; the damage of fibers as a whole; the transverse damage of matrix; the in-plane damage of matrix; and delamination damage. For illustrative purposes,

an example of 8.5mm thickness target made of 3D orthogonal woven composite and subjected to a bullet impact at a velocity of 699m/s is presented. This example is to show the damage evolution of *x*-fiber and the in-plane damage of matrix.

A. Damage of *x*-fiber

Figure 11 is the damage evolution of *x*-fiber at six different instants. At the beginning of impact (at $3ms$), the fibers which are in contact with the bullet suffer both compression and shear. These fibers fail in a form of compression/shear damage. As penetration goes on, the transverse compressive wave reflects at the back side to create a transverse tensile wave, which subsequently causes fiber damage near the back side (at $9ms$). The damage evolves as penetration progresses (at $12ms$). The fibers fail absolutely when the damage accumulates to a limit of 1. The fibers near the back suffer tensile failure (at $18ms$). Finally fracture of target occurs and the fragments of fibers escapes (at $24ms$, $30ms$).

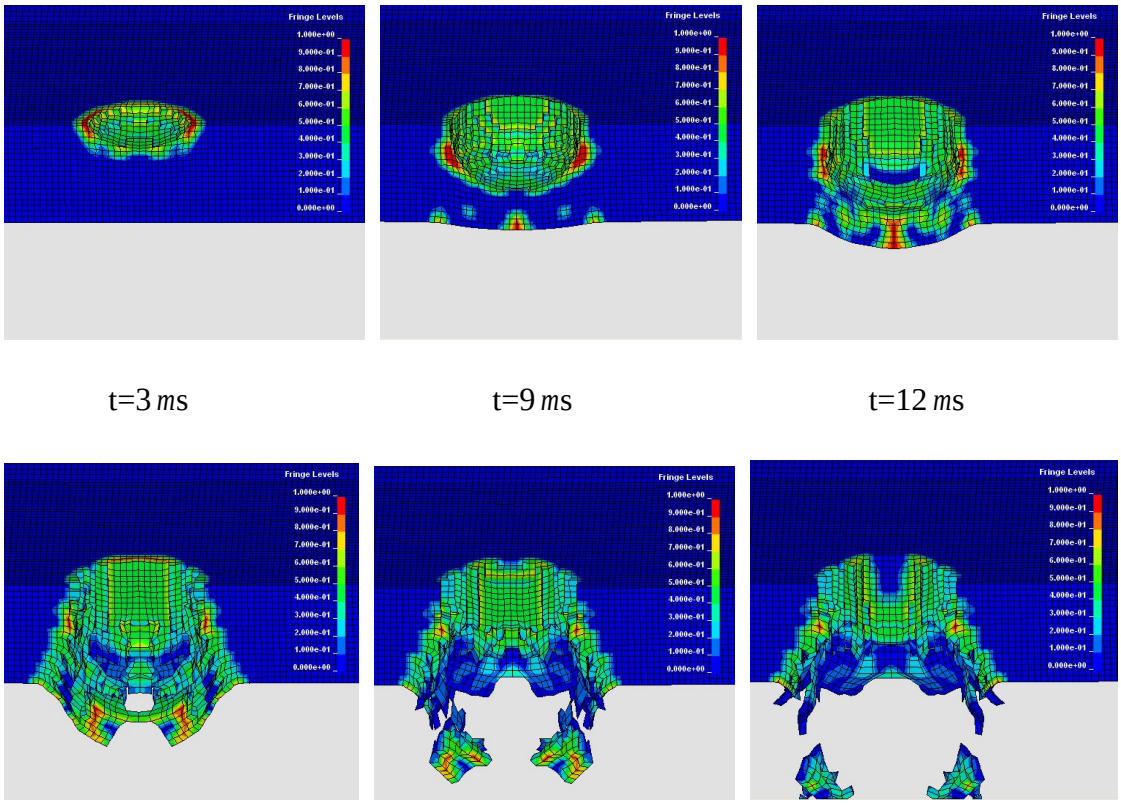

Fig.11 Damage of *x*-fiber at different instants

From the evolution of damage distribution, there are two obvious damage areas, the compression/shear damage failure in the vicinity of the impact side, and the tensile damage in

the vicinity of the back side.

B. In-plane damage of matrix

The evolution of in-plane damage of matrix can be seen in Fig. 12. At the beginning of penetration, the area which is in contact with the bullet suffers compressive damage (at $6ms$). As the compressive wave propagates transversely, it causes more damage to the matrix because of low matrix strength (at $9ms$). The tensile wave reflected from the back side results in a worse situation where more matrix reach its damage limit. Ultimately, the matrix fails with some fragments even ejected (at $18,\ 21,\ 24ms$). Because of considerably lower strength as compared to fibers, fragments of matrix escape first prior to the escape of fragments of fibers.

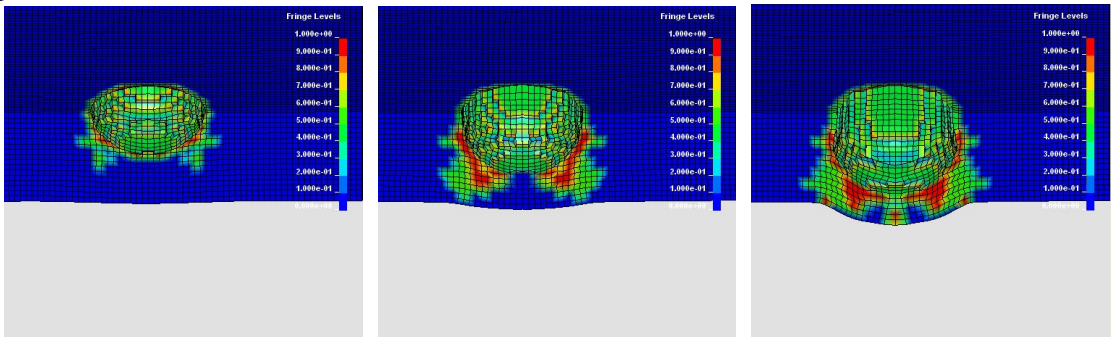

t=6 *ms* t=9 *ms* t=12 *ms*

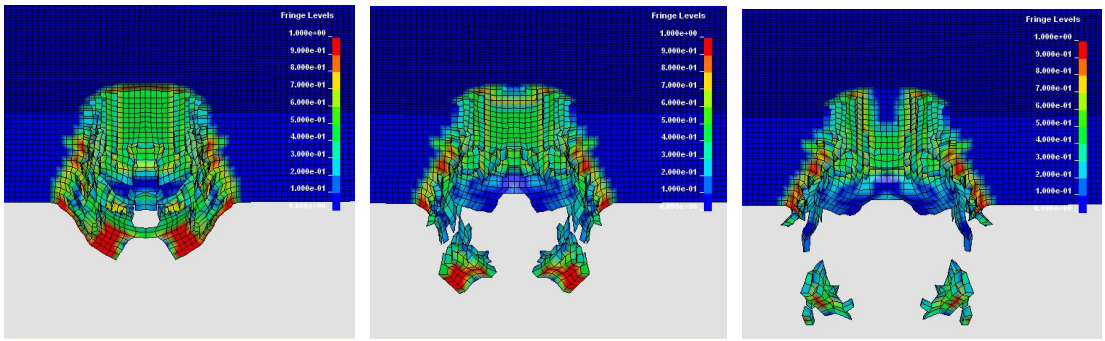

t=18 *ms* t=24 *ms* t=30 *ms*

Fig.12. Damage of inter-face at different instants

7. Conclusions

This paper presents a ballistic impact experiment and simulation for 3D orthogonal woven composite. A detailed investigation of two new materials, Kevlar/Vinyl and E-glass/Vinyl with no known investigation a priori, subjected to an impact by a spherical bullet is presented herein. The essence and significant contribution of this paper are its in-depth analysis of the main energy absorption mechanism and the effect of Z yarns to the damage modes for 3D-OWC. In addition, the whole process of damage evolution is also

described in detail and simulated by finite element analysis.

Meanwhile, there are a few significant conclusions in this paper. From the experiment, it concludes that the BPI of Kevlar/Vinyl 3D-OWC is higher than that of E-glass/Vinyl, which means that the former has better ballistic performance than the latter. The failure of 3D-OWC also indicates an obvious fiber and matrix damage area of twice the diameter of the bullet. The compression/shearing failure is observed as the main cause failure on the impact side whiles tensile failure is significant on the back side. Analysis of the energy absorption mechanism points out that Z yarns significantly enhances the in-plane strength of 3D-OWC as compared to equivalent laminates. The existence of Z yarns also makes delamination and conical bulge of 3D-OWC impossible. The experiment concludes that the in-plane energy absorption mechanism is the main mechanism.

The paper also presents numerical simulations using finite elements. The residual velocities determined from FE simulation are fitted to the experiment measurement. The time history of penetration velocity indicates a finite steady process penetration. The damage evolution of *x*-fibers and in-plane matrix are given in this paper, and they point out that there exists a compression/shear damage area in the vicinity of the impact side and a tensile damage area in the vicinity of the back side, which are consistent with experiment observation.

Acknowledgements

The work described in this paper was supported by National Science Foundation of China [10572134] and City University of Hong Kong [Project No. 7002357 (BC)].

References

1. Antonio, M., *3D textile reinforcements in composite materials*, CRC Press, London, 1999.
2. Baucom, J.N., Zikry, M.A., Evolution of Failure Mechanisms in 2D and 3D woven composite systems under quasi-static perforation, *J. Compos Mater.*, 37, 1651-1674, 2003.
3. Baucom, J.N., Zikry, M.A., Low-velocity impact damage progression in woven E-glass composite systems, *Compos. Pt. A.*, 36, 658-664, 2005.
4. Tan, P., Tong, L., Steven, G.P., and Takashi, I., Behavior of 3D orthogonal woven CFRP composites Part 1. Experimental investigation, *Compos. Pt. A.*, 31, 259-271, 2000.
5. Tan, P., T, L., and Steven, G.P., Behavior of 3D orthogonal woven CFRP composites Part 2. FEA and analytical modeling approaches, *Compos. Pt. A.*, 31, 273-281, 2000.
6. Tan, P., Tong, L., and Steven, G.P., Mechanical behavior for 3D orthogonal woven E-glass/expoxy composites, *J Reinf. Plast. Compos.*, 20, 274-303, 2001.
7. Tan, P., Tong, L., and Steven, G.P., Modeling approaches for 3D orthogonal woven composites, *J Reinf Plast Compos*, 17, 545-577, 1998.
8. Tan, P., Tong, L., and Steven, G.P., Models for predicting thermo-mechanical properties of three dimensional orthogonal woven composites, *J Reinf Plast Compos.*, 18, 151–85, 1999.
9. Tong, L,, Tan, P., and Steven, G.P., Effect of yarn waviness on strength of 3D orthogonal woven CFRP composite materials, *J Reinf Plast. Compos.*, 21, 153-173, 2002.
10. Shahkarami, A., Vaziri, R., A continuum shell finite element model for impact simulation of woven

fabrics, *Int. J. Impact Eng.*, 34, 104-119, 2007.
11. Rudov-Clark, S., Mouritz, A.P., Tensile fatigue properties of a 3D orthogonal woven composite, *Compos. Pt. A.*, 39, 1018-1024, 2008.
12. Callus, P.J., Mouritz, A.P., Bannister, M.K., and Leong, K.H., Tensile properties and failure mechanisms of 3D woven GRP composites, *Compos. Pt. A.*, 30, 1277-1287, 1999.
13. Quinn, J.P., McIlhagger, A.T., and McIlhagger, R., Examination of the failure of 3D woven composites, *Compos. Pt. A.*, 39, 273-283, 2008.
14. Lv., L.H., Sun, B.Z., Qiu, Y.P., and Gu, B.H., Energy absorption and failure modes of 3D orthogonal hybrid woven composite struck by flat-ended rod, *Polym. Compos.*, 27, 411-416, 2006.
15. Lv, L.H., Gu, B.H., Transverse Impact Damage and Energy Absorption of Three-Dimensional Orthogonal Hybrid Woven Composite: Experimental and FEM Simulation, *J. Compos Mater.*, 42, 1763-1786, 2008.
16. Luo, Y.S., Lv, L.H., Sun, B.Z., Qiu, Y.P., and Gu, B.H., Transverse impact behavior and energy absorption of three-dimensional orthogonal hybrid woven composite, *Compos. Struct.*, 81, 202-209, 2007.
17. Naik, N.K., Azad, S.N.M., Prasad, P.D., and Thuruthimattam, B.J., Stress and failure analysis of 3D orthogonal interlock woven composites, *J. Reinf. Plast. Compos.*, 20, 1485–523, 2001.
18. Naik, N.K., Sridevi, E., An analytical method for thermoelastic analysis of 3D orthogonal interlocks woven composites, *J. Reinf. Plast. Compos.*, 21, 1149–91, 2002.
19. Naik, N.K., Shrirao, P., Composite structures under ballistic impact, *Compos. Struct.*, 66, 579-590, 2004.
20. Naik, N.K., Venkateswara, R.K., High strain rate behavior of woven fabric composites under compressive loading, *Mater. Sci. Eng. A.*, 474, 301-311, 2008.
21. Karim, M.R., Constitutive modeling and failure criteria of carbon-fiber reinforced polymers under high strain rates, PhD dissertation, University of Akron, 2005.
22. Tan, V.B.C., Ching, T.W., Computational simulation of fabric armor subjected to ballistic impacts, *Int. J. Impact Eng.*, 32, 1737-1751, 2006.
23. Gama, B.A., Haque, Md. J., Gillespie, J.W. Jr., and Bogdanovich, A.E., Impact, Damage, and Energy Absorption of a 3D Orthogonal Weave Composite Unit Cell Model, *Proceedings of the SAMPE 2004 Symposium*, Long Beach, CA, May, 16-20, 2004
24. Gama, B.A., Bogdanovich, A.E., Md. J., and Gillespie, J.W. Jr., Ballistic impact damage modeling and experimental validation on a 3-D orthogonal weave fabric composite, *Proceedings of SAMPE 2005 Symposium & Exhibition (50th ISSE)*, Long Beach, CA, May, 1-5, 2005.
25. *LS-DYNA THEORETICAL MANUAL*, Livermore Software Technology Corporation, May, 1998.
26. *LS-DYNA KEYWORD USER'S MANUAL*, Livermore Software Technology Corporation, April, 2003.
27. Yen, C.F., Caiazzo, A., Innovative processing of multifunctional composite armor for ground vehicles, ARL-CR-484, U.S. Army Research Laboratory, Aberdeen ProVing Ground, MD, 2001.